Normal Modes of Metallochlorins Revisited: Comparison of Force Fields and Factors Influencing the Vibrational Eigenvectors

Alexander D. Procyk,[†] Younkyoo Kim,[‡] Einhard Schmidt,[‡] Harold N. Fonda,[‡,§] Chi-Kwong Chang,[‡] Gerald T. Babcock,*[,‡] and David F. Bocian*[,†]

Contribution from the Department of Chemistry, University of California, Riverside, California 92521, and Department of Chemistry and the LASER Laboratory, Michigan State University, East Lansing, Michigan 48824. *Received January 31, 1992*

Abstract: Empirical normal coordinate calculations are reported for the Cu(II) complex of octaethylchlorin (OEC) and a series of *meso*-deuteriated isotopomers, including CuOEC-α,β-d_2, CuOEC-γ,δ-d_2, and CuOEC-d_4. The deuteriation in these isotopomers systematically perturbs each of the symmetry inequivalent methine bridges of the OEC ring. The calculations indicate that various force fields satisfactorily reproduce the general features and the vibrational spectra of CuOEC. However, none of these force fields reproduce the frequencies and *meso*-deuteriation shift patterns of all of the modes. All of the empirical force fields predict that the eigenvectors of certain skeletal modes are localized on sectors of the macrocycle. This localization does not depend on the detailed aspects of the force field and is a general consequence of symmetry lowering. This conclusion is substantiated by additional data obtained for ZnOEC, which show that the *meso*-deuteriation shift patterns of the skeletal modes of this complex are virtually the same as those of CuOEC. The prediction that certain vibrational eigenvectors of MOEC complexes are localized is in accord with the results of previous studies of these complexes in which semiempirical methods were used to generate the eigenvectors. Quantitative comparison of the empirical and semiempirical force fields indicates that 1,4 and higher interaction constants make substantial contributions to the latter force fields. These interactions are not included in the empirical force field calculations. Accordingly, the values of the force constants used in the empirical calculations are not necessarily repesentative of the actual force field effective in the macrocycle. Collectively, these studies indicate that both empirical and semiempirical normal coordinate calculations give a reasonable estimate of the forms of the vibrational eigenvectors of the MOEC complexes.

Introduction

Hydroporphyrins serve as the prosthetic groups in a variety of proteins that participate in electron transfer and catalysis.[1-29] The structural and electronic properties of these macrocycles determine the detailed aspects of their functional nature. The vibrational characteristics of the ring are a particularly sensitive indicator of these properties (for a review, see ref 30). Accordingly, we and others have been using vibrational spectroscopy to probe hydroporphyrins and related macrocycles.[31-53] At present, a substantial body of vibrational data is available for reduced-pyrrole macrocycles. Most of these data have been acquired for metallodihydroporphyrins (metallochlorins). These macrocycles are structurally the most similar to metalloporphyrins in that only one of the four pyrrole rings is reduced (Figure 1).

The availability of a considerable amount of vibrational data for metallodihydroporphyrins makes these rings the most amenable to vibrational analysis. The first interpretations of the vibrational spectra of these systems were made exclusively by analogy to those of metalloporphyrins.[23,31-35] This type of analysis presumes that the vibrational eigenvectors of the two different classes of macrocycles are similar. Because there is no a priori basis for this assumption, normal coordinate analyses are required to delineate the exact forms of the normal modes of the reduced-pyrrole systems. In this regard, normal coordinate calculations have been reported for a variety of metallodihydroporphyrins, including nickel(II) octaethylchlorin (NiOEC),[37,41] copper(II) tetraphenylchlorin,[40] and several nickel(II) pheophorbides.[37] Our group has examined all of these species by using semiempirical quantum force field and/or empirical force field (**FG** matrix) methods.[37,40] Several other groups have also examined MOEC complexes by using empirical force field methods.[36,41] Our calculations (both empirical and semiempirical) predict that the forms of the normal modes of metallodihydroporphyrins are in general different from those of porphyrins. In contrast, empirical calculations on NiOEC by Prendergast and Spiro predict that the vibrational eigenvectors of metallochlorins are similar to those of metalloporphyrins.[41]

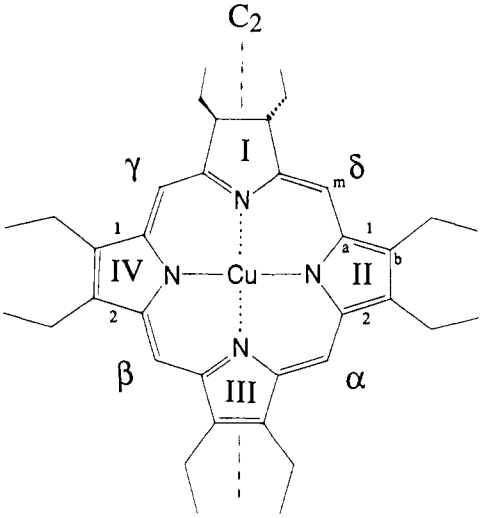

Figure 1. Structure and labeling scheme for CuOEC.

[†] University of California.
[‡] Michigan State University.
[§] Present address: Department of Chemistry, Colorado State University, Fort Collins, CO 80523.

(1) Svec, W. A. In *The Porphyrins*; Dolphin, D., Ed.; Academic Press: New York, 1978; Vol. 5, pp 341-349.
(2) Babcock, G. T.; Ingle, R. T.; Oertling, W. A.; Davis, J. C.; Averill, B. A.; Hulse, C. L.; Stufkens, D. J.; Bolscher, B. G. J. M.; Wever, R. *Biochim. Biophys. Acta* **1985**, *828*, 58-66.
(3) Sibbet, S. S.; Hurst, J. K. *Biochemistry* **1984**, *23*, 3007-3013.
(4) Eglington, D. G.; Barber, D.; Thomson, A. J.; Greenwood, C.; Segal, A. W. *Biochim. Biophys. Acta* **1982**, *703*, 187-195.
(5) Morell, D. B.; Chang, Y.; Henry, I.; Nichol, A. W.; Clezy, P. S. In *Structure and Function of Cytochromes*; Okunuki, K., Kamen, M. D., Sekuzu, I., Eds.; University Park Press: Baltimore, 1968; pp 563-571.
(6) Morell, D. B.; Chang, Y.; Clezy, P. S. *Biochim. Biophys. Acta* **1967**, *136*, 121-130.
(7) Newton, N.; Morell, D. B.; Clarke, L. *Biochim. Biophys. Acta* **1965**, *96*, 463-475.

0002-7863/92/1514-6539$03.00/0

The origin of the disparities between the empirical and semiempirical normal coordinate calculations on NiOEC is uncertain, although Spiro and co-workers have suggested that they are due to intrinsic inaccuracies in the semiempirical approach.[41] While it is true that semiempirical vibrational analysis methods are less accurate than empirical approaches, the development of an accurate empirical force field requires data from a variety of isotopomers. At the time of our original work, detailed vibrational data were available for only a single isotopomer of NiOEC, specifically the *meso*-deuteriated species NiOEC-γ,δ-d_2 (limited data were also available for CuOEC-$^{15}N^{31}$). This limited amount of isotope data is not sufficient to develop an accurate empirical force field; therefore, we chose a semiempirical approach. In their recent empirical normal coordinate calculations on NiOEC, Prendergast and Spiro utilized the vibrational data from NiOEC-γ,δ-d_2 supplemented only by new information from the pyrrole-^{15}N isotopomer.[41] No new *meso*-deuteriation data were included in the calculations. The inclusion of additional *meso*-deuteriation data is essential for the development of an accurate force field, because the deuteriation in NiOEC-γ,δ-d_2 samples only one of the two symmetry inequivalent methine bridges in the macrocycle (Figure 1).

Recently one of our groups obtained detailed infrared (IR) and resonance Raman (RR) data for a series of *meso*-deuteriated CuOEC complexes.[42] These complexes included CuOEC-α,β-d_2, CuOEC-γ,δ-d_2, and CuOEC-d_4. The deuteriation in these isotopomers systematically perturbs each of the symmetry inequivalent methine bridges of the OEC ring. The availability of these data prompted us to develop an empirical force field for CuOEC. An additional motivation for using CuOEC for the calculations derives from the fact that in this complex the ring is less perturbed by ruffling and saddling than is the ring in NiOEC.[54] In the course of our investigation, vibrational data were also acquired for the Zn(II) complexes of the various *meso*-deuteriated isotopomers. These data allow the examination of the effects of the central metal ion on the forms of the vibrational eigenvectors. Collectively, this new information provides a basis for a comparison of the various force fields for MOEC complexes and the factors that influence the forms of the vibrational eigenvectors.

Methods

Experimental Procedures. *trans*-OEC was prepared by the method of Whitlock et al.[55] Following the reduction, residual porphyrin was removed by alumina column chromatography with benzene as eluent. The *meso*-deuteriated isotopomers OEC-α,β-d_2, OEC-γ,β-d_2, and OEC-d_4 were prepared as previously reported.[42] The deuteriation process was followed and confirmed by ^{1}H NMR by using a Varian VXR-3005 NMR spectrometer. Metal insertion was achieved by dissolving OEC in CH_2Cl_2 and adding an appropriated volume of saturated Zn(II) or Cu(II) acetate in CH_3OH. The process was followed by UV–vis spectroscopy by using a Shimadzu UV-160 spectrometer.

Infrared spectra were recorded at room temperature on a Nicolet IR/42 FTIR spectrometer. Samples were prepared by saturating $CHCl_3$ with the various MOEC complexes and were contained in a 50 μm path length NaCl cavity cell (Spectra Tech, Inc.).

Resonance Raman spectra were obtained at room temperature with 5-cm^{-1} resolution on a Spex 1877 B equipped with a EG&G Model 1421 detector and an OMAIII controller for data acquisition and analysis.

(8) Newton, N.; Morell, D. B.; Clarke, L.; Clezy, P. S. *Biochim. Biophys. Acta* **1965**, *96*, 476–486.
(9) Chang, C. K. *J. Biol. Chem.* **1985**, *260*, 9520–9522.
(10) Lemberg, R.; Barret, J. *Cytochromes*; Academic Press: New York, 1973; pp 233–245.
(11) Chatfield, M. J.; La Mar, G. M.; Smith, K. N.; Leung, H.-K.; Pandy, R. K. *Biochemistry* **1965**, *27*, 1500–1507.
(12) Bondoc, L. L.; Chau, M.-H.; Price, M. A.; Timkovich, R. *Biochemistry* **1986**, *25*, 8458–8466.
(13) Chatfield, M. J.; La Mar, G. N.; Lecomte, J. T. J.; Balch, A. L.; Smith, K. M.; Langry, K. C. *J. Am. Chem. Soc.* **1986**, *108*, 7108–7110.
(14) Andersson, L. A.; Loehr, T. M.; Lim, A. R.; Mauk, A. G. *J. Biol. Chem.* **1984**, *259*, 15340–15349.
(15) Peisach, J.; Blumberg, W. E.; Adler, A. *Ann. N.Y. Acad. Sci.* **1973**, *206*, 310–327.
(16) Berofsky, J. A.; Peisach, J.; Blumberg, W. E. *J. Biol. Chem.* **1971**, *246*, 3367–3377.
(17) Brittain, T.; Greenwood, C.; Barber, D. *Biochim. Biophys. Acta* **1982**, *705*, 26–32.
(18) Okamura, M. Y.; Feher, G.; Nelson, N. In *Photosynthesis*; Godvindjee, Ed.; Academic Press: New York, 1982; Vol. I, pp 195–272.
(19) Feher, G.; Okamura, M. Y. In *The Photosynthetic Bacteria*; Clayton, R. K., Sistron, W. R., Eds.; Plentum Press: New York, 1978; pp 349–386.
(20) Lancester, J. R.; Vega, J. M.; Kamin, H.; Orme-Johnson, N. R.; Orme-Johnson, W. H.; Kreuger, R. H.; Siegel, L. M. *J. Biol. Chem.* **1979**, *254*, 1268–1272.
(21) Vega, J. M.; Kamin, H. *J. Biol. Chem.* **1977**, *252*, 896–909.
(22) Murphy, M. J.; Siegel, L. M.; Tover, S. R.; Kamin, H. *Proc. Natl. Acad. Sci. U.S.A.* **1974**, *71*, 612–616.
(23) Andersson, L. A.; Sotiriou, C.; Chang, C. K.; Loehr, T. M. *J. Am. Chem. Soc.* **1987**, *109*, 258–264.
(24) Scott, A. I.; Irwin, A. J.; Siegel, J. M.; Schoolery, J. N. *J. Am. Chem. Soc.* **1978**, *100*, 316–318, 7987–7994.
(25) Siegel, J. M.; Rueger, D. C.; Barber, M. J.; Krueger, R. J.; Orme-Johnson, N. R.; Orme-Johnson, W. H. *J. Biol. Chem.* **1982**, *257*, 6343–6350.
(26) McRee, D. E.; Richardson, D. C.; Richardson, J. S.; Siegel, L. M. *J. Biol. Chem.* **1986**, *261*, 10277–10281.
(27) Wolfe, R. S. *Trends Biochem. Sci. Presonal Ed.* **1985**, *10*, 369–399.
(28) Ellefson, W. L.; Whitman, W. B.; Wolfe, R. S. *Proc. Natl. Acad. Sci. U.S.A.* **1982**, *79*, 3707–3710.
(29) Pfaltz, A.; Juan, B.; Fassler, A.; Eschenmoser, A.; Jaenchen, R.; Gilles, H. H.; Diekert, G.; Thauer, R. K. *Helv. Chim. Acta* **1982**, *65*, 828–865.
(30) Schick, G. A.; Bocian, D. F. *Biochim. Biophys. Acta* **1987**, *895*, 127–154.
(31) Ozaki, Y.; Kitagawa, T.; Ogoshi, H. *Inorg. Chem.* **1979**, *18*, 1772–1776.
(32) (a) Ozaki, Y.; Iriyama, K.; Ogoshi, H.; Ochiai, T.; Kitagawa, T. *J. Phys. Chem.* **1986**, *90*, 6105–6112. (b) Ozaki, Y.; Iriyama, K.; Ogoshi, H.; Ochiai, T.; Kitagawa, T. *J. Phys. Chem.* **1986**, *90*, 6113–6118.
(33) (a) Fujiwara, M.; Tasumi, M. *J. Phys. Chem.* **1986**, *90*, 250–255. (b) Fujiwara, M.; Tasumi, M. *J. Phys. Chem.* **1986**, *90*, 5646–5650.
(34) Andersson, L. A.; Loehr, T. M.; Cotton, T. M.; Simpson, D. J.; Smith, K. M. *Biochim. Biophys. Acta* **1989**, *974*, 163–179.
(35) (a) Andersson, L. A.; Loehr, T. M.; Chang, C. K.; Mauk, A. G. *J. Am. Chem. Soc.* **1985**, *107*, 182–191. (b) Andersson, L. A.; Loehr, T. M.; Sotiriou, C.; Wu, W.; Chang, C. K. *J. Am. Chem. Soc.* **1986**, *108*, 2908–2916.
(36) Gladkov, L. L.; Starukhin, A. S.; Shulga, A. M. *Spectrochim. Acta* **1987**, *43A*, 1125–1134.
(37) Boldt, N. J.; Donohoe, R. J.; Birge, R. R.; Bocian, D. F. *J. Am. Chem. Soc.* **1987**, *109*, 2284–2298.
(38) Boldt, N. J.; Bocian, D. F. *J. Phys. Chem.* **1988**, *92*, 581–586.
(39) Ogoshi, H.; Watanabe, E.; Yoshida, Z.; Kincaid, J.; Nakamoto, K. *Inorg. Chem.* **1975**, *14*, 1344–1350.
(40) Donohoe, R. J.; Atamian, M.; Bocian, D. F. *J. Phys. Chem.* **1989**, *93*, 2244–2252.
(41) Prendergast, K.; Spiro, T. G. *J. Phys. Chem.* **1991**, *95*, 1555–1563.
(42) Fonda, H. N.; Oertling, W. A.; Salehi, A.; Chang, C. K.; Babcock, G. T. *J. Am. Chem. Soc.* **1990**, *112*, 9497–9507.
(43) (a) Lutz, M. In *Advances in Infrared and Raman Spectroscopy*; Clark, R. J. H., Hester, R. E., Eds.; Wiley: New York, 1984; Vol. 11, pp 211–300. (b) Lutz, M.; Robert, B. In *Biological Applications of Raman Spectroscopy*; Spiro, T. G., Ed.; Wiley: New York, 1988; Vol. III, pp 347–411.
(44) (a) Cotton, T. M.; Van Duyne, R. P. *J. Am. Chem. Soc.* **1981**, *103*, 6020–6026. (b) Callahan, P. M.; Cotton, T. M. *J. Am. Chem. Soc.* **1987**, *109*, 7001–7007.
(45) Donohoe, R. J.; Frank, H. A.; Bocian, D. F. *Photochem. Photobiol.* **1988**, *48*, 531–537.
(46) Cotton, T. M.; Timkovich, R.; Cork, M. S. *FEBS Lett.* **1981**, *133*, 39–44.
(47) Ching, Y.; Ondrias, M. R.; Rosseau, D. L.; Muhoberac, B. B.; Wharton, D. C. *FEBS Lett.* **1982**, *138*, 239–244.
(48) (a) Andersson, L. A.; Loehr, T. M.; Wu, W.; Chang, C. K.; Timkovich, R. *FEBS Lett.* **1990**, *267*, 285–288. (b) Mylrajan, M.; Andersson, L. A.; Loehr, T. M.; Wu, W.; Chang, C. K. *J. Am. Chem. Soc.* **1991**, *113*, 5000–5005.
(49) Andersson, L. A.; Loehr, T. M.; Thompson, R. G.; Strauss, S. H. *Inorg. Chem.* **1990**, *29*, 2142–2147.
(50) Ondrias, M. R.; Carson, S. D.; Hirasawa, M.; Knaff, D. B. *Biochim. Biophys. Acta* **1985**, *830*, 159–163.
(51) (a) Han, S.; Madden, J. F.; Thompson, R. G.; Strauss, S. H.; Siegel, L. M.; Spiro, T. G. *Biochemistry* **1989**, *28*, 5461–5470. (b) Melamed, D.; Sullivan, E. P.; Prendergast, K.; Strauss, S. H.; Spiro, T. G. *Inorg. Chem.* **1991**, *30*, 1308–1319.
(52) (a) Lai, K. K.; Yue, K. T. *J. Raman Spectrosc.* **1990**, *21*, 21–26. (b) Lai, K. K.; Moura, I.; Liu, M. Y.; LeGall, J.; Yue, K. T. *Biochim. Biophys. Acta* **1991**, *1060*, 25–27.
(53) (a) Bocian, D. F.; Procyk, A. D.; Peloquin, J. M. *Proc. SPIE* **1989**, *1057*, 146–153. (b) Procyk, A. D.; Bocian, D. F. *J. Am. Chem. Soc.* **1991**, *113*, 3765–3773.
(54) (a) Stolzenberg, A. M.; Stershic, M. T. *Inorg. Chem.* **1987**, *26*, 1970–1977. (b) Stolzenberg, A. M.; Stershic, M. T. *J. Am. Chem. Soc.* **1988**, *110*, 6391–6402.
(55) Whitlock, H. W., Jr.; Hanauer, R.; Oester, M. Y.; Bower, B. K. *J. Am. Chem. Soc.* **1969**, *91*, 7485–7489.

Table I. Geometric Parameters for CuOEC

	FG	QCFF/PI[a]		FG	QCFF/PI[a]
		Bond Lengths			
Cu–N(I)	1.979	2.092	$C_a(II_1)$–$C_m(\delta)$	1.401	1.429
Cu–N(II)	1.973	2.061	$C_a(II_2)$–$C_m(\alpha)$	1.363	1.378
Cu–N(III)	1.956	2.065	$C_a(III)$–$C_m(\alpha)$	1.401	1.426
N(I)–C_a(I)	1.327	1.347	$C_b(I)$–$C_b(I)$	1.433	1.493
N(II)–$C_a(II_1)$	1.370	1.348	$C_b(II_1)$–$C_b(II_2)$	1.351	1.392
N(II)–$C_a(II_2)$	1.389	1.387	$C_b(III)$–$C_b(III)$	1.346	1.415
N(III)–C_a(III)	1.379	1.369	$C_m(\delta)$–H	1.100	1.088
$C_a(I)$–$C_b(I)$	1.502	1.576	$C_m(\alpha)$–H	1.100	1.086
$C_a(II_1)$–$C_b(II_1)$	1.437	1.431	$C_b(I)$–$C_1(I)$	1.488	1.459
$C_a(II_2)$–$C_b(II_2)$	1.446	1.453	$C_b(II_1)$–$C_1(II_1)$	1.505	1.459
C_a(III)–C_b(III)	1.433	1.416	$C_b(II_2)$–$C_1(II_2)$	1.501	1.459
$C_a(I)$–$C_m(\delta)$	1.363	1.359	C_b(III)–C_1(III)	1.506	1.455
		Bond Angles			
N(I)–Cu–N(II)	89.2	89.8	$C_a(II_2)$–$C_b(II_2)$–$C_b(II_1)$	106.0	106.3
N(II)–Cu–N(III)	90.8	90.2	C_a(III)–C_b(III)–C_b(III)	107.0	106.6
$C_a(I)$–N(I)–$C_a(I)$	100.5	109.9	N(I)–$C_a(I)$–$C_m(\delta)$	122.9	127.7
$C_a(II_1)$–N(II)–$C_a(II_2)$	105.0	108.8	N(II)–$C_a(II_1)$–$C_m(\delta)$	124.4	126.5
C_a(III)–N(III)–C_a(III)	104.7	108.7	N(II)–$C_a(II_2)$–$C_m(\alpha)$	124.4	127.5
N(I)–$C_a(I)$–$C_b(I)$	119.5	111.9	N(III)–C_a(III)–$C_m(\alpha)$	124.4	127.0
N(II)–$C_a(II_1)$–$C_b(II_1)$	110.6	109.7	Cu–N(I)–$C_a(I)$	131.2	125.0
N(II)–$C_a(II_2)$–$C_b(II_2)$	110.6	108.0	Cu–N(II)–$C_a(II_1)$	127.6	125.6
N(III)–C_a(III)–C_b(III)	110.6	109.0	Cu–N(II)–$C_a(II_2)$	127.4	125.5
$C_a(I)$–$C_m(\delta)$–$C_a(II_1)$	125.4	125.2	Cu–N(III)–C_a(III)	127.6	125.6
$C_a(II_2)$–$C_m(\alpha)$–C_a(III)	125.4	124.1	$C_m(\delta)$–$C_a(I)$–$C_b(I)$	117.6	120.3
$C_a(I)$–$C_b(I)$–$C_1(I)$	112.9	109.8	$C_m(\delta)$–$C_a(II_1)$–$C_b(II_1)$	125.0	123.8
$C_a(II_1)$–$C_b(II_1)$–$C_1(II_1)$	124.6	126.4	$C_m(\alpha)$–$C_a(II_2)$–$C_b(II_2)$	125.0	123.9
$C_a(II_2)$–$C_b(II_2)$–$C_1(II_2)$	125.1	126.6	$C_m(\alpha)$–C_a(III)–C_b(III)	125.0	123.9
C_a(III)–C_b(III)–C_1(III)	124.8	127.1	$C_b(I)$–$C_b(I)$–$C_1(I)$	130.2	125.8
$C_a(I)$–$C_b(I)$–$C_b(I)$	100.9	103.1	$C_b(II_1)$–$C_b(II_2)$–$C_1(II_2)$	128.8	127.1
$C_a(II_1)$–$C_b(II_1)$–$C_b(II_2)$	107.7	107.2	$C_b(II_2)$–$C_b(II_1)$–$C_1(II_1)$	127.6	126.4
			C_b(III)–C_b(III)–C_1(III)	128.2	126.3

[a] Point mass calculation (see text).

Excitation at 406.7 nm was provided by an Coherent Innova 90 krypton ion laser. Spectra were obtained of the MOEC complexes in CH_2Cl_2 solutions contained in a cylindrical quartz spinning cell. Spectra were collected within 1 min of initiating laser irradiation in order to minimized demetalation and/or sample decomposition. UV–vis spectra were recorded before and after the Raman measurements to confirm the integrity of the samples. The laser power and sample concentrations used for specific measurements are noted in the figure legends.

Normal Coordinate Calculations. The first set of normal coordinate calculations for CuOEC was performed by using the semiempirical quantum chemistry force field (QCFF/PI) method of Warshel and Karplus.[56] The details of these calculations are the same as those described in Boldt et al.[37] One set of calculations was performed with the ethyl groups included as 15 amu point masses. Another set was performed with the ethylene carbons and hydrogens explicitly included and the terminal methyl groups approximated as 15 amu point masses. In this calculation, the methyl groups were positioned above and below the plane of the macrocycle such that C_2 symmetry was preserved. The configuration of these groups is the same as that used by Prendergast and Spiro in their empirical calculations.[41] The QCFF/PI procedure produces an optimized structure in the course of energy minimization. The bond lengths and bond angles of the ring skeleton obtained for the ethyl point mass calculation are listed in Table I. These structural parameters are essentially unaltered when the ethyl groups are included.

The second set of normal coordinate calculations for CuOEC was performed by using the empirical **FG** matrix method of Wilson.[57] The **G** matrix was constructed by using the crystallographic data for FeOEC.[58] This structure was also used by Prendergast and Spiro in their normal coordinate calculations on NiOEC. The crystallographically determined structure of the FeOEC ring skeleton is nonplanar and deviates somewhat from C_2 symmetry. In our calcualtions, the geometry was adjusted to give a planar, C_2 structure. The ethyl groups were explicitly included in the empirical calculations as described above for the QCFF/PI studies. The bond lengths and bond angles of the ring skeleton in this idealized structure are given in Table I.

The empirical normal coordinate calculations for CuOEC were initiated by constructing the **F** matrix reported for NiOEC by Prendergast and Spiro.[41] This force field for NiOEC was developed via a selective refinement of the valence force field previously developed for nickel(II) octaethylporphyrin.[59] In constructing the force field for CuOEC, we noted that the 1,3 C_aC_m–C_bC_b interaction constants were omitted from the off-diagonal force constants listed for NiOEC in ref 41. We presume this was an oversight in the tabulation rather than in the calculation because omission of this interaction constant results in overestimation of the *meso*-deuteriation shifts for the C_bC_b stretches. More importantly, we noted that the magnitude of the diagonal C_aC_m force constants tabulated in ref 41 follows a pattern that would correspond to a long–short–long–short alteration of the C_aC_m bond lengths (starting from the reduced ring) rather than the actual short–long–short–long pattern.[58,60,61] We initially assumed that this was also an oversight in tabulation; however, calculations performed with the C_aC_m force constants in both the order consistent with the bond lengths and the reversed (tabulated) order revealed that the latter actually yielded *meso*-deuteriation shifts for NiOEC-γ,δ-d_2 that are in better accord with the calculated values reported in ref 41. Regardless of the ordering used for the C_aC_m force constants, we were unable to reproduce a number of the calculated *meso*-deuteriation shifts for NiOEC-d_4, particularly the large shifts reported for ν_{10} (18 cm^{-1}) and ν_{19} (29 cm^{-1}). All attempts to determine the origin of the discrepancies between our calculations and those reported in ref 41 were unsuccessful.

Our initial calculations on CuOEC utilized the **F** matrix constructed for NiOEC with the C_aC_m force constants ordered consistent with the bond lengths. As expected, this force field overestimates the vibrational frequencies for a number of the skeletal modes of CuOEC. [The skeletal-mode frequencies of NiOEC (for which the force field was refined) are in general higher than those of CuOEC.[37,41,42]] Consequently, we systematically reduced the magnitude of all the diagonal stretching force constants (excluding those of the ethyl groups and the C_mH bonds) before

(56) (a) Warshel, A.; Karplus, M. *J. Am. Chem. Soc.* **1972**, *94*, 5612–5625. (b) Warshel, A.; Levitt, M. *Quantum Chemistry Program Exchange* **1974**, *No. 247*.

(57) Schachtschneider, J. H. *Vibrational Analysis of Polyatomic Molecules*; Shell Development Co.: Emeryville, CA, 1962; Vols. I–III.

(58) Strauss, S. H.; Silver, M. E.; Long, K. M.; Thompson, R. G.; Hudgens, R. A.; Spartalian, K.; Ibers, J. A. *J. Am. Chem. Soc.* **1985**, *107*, 4207–4215.

(59) Li, X.-Y.; Czernuszewicz, R. S.; Kincaid, J. R.; Stein, P.; Spiro, T. G. *J. Phys. Chem.* **1990**, *94*, 47–61.

(60) Spaulding, L. D.; Andrews, L. C.; Williams, G. J. D. *J. Am. Chem. Soc.* **1977**, *99*, 6918–6923.

(61) Gallucci, J. C.; Swepston, P. N.; Ibers, J. A. *Acta Crystallogr. Sect. B: Struct. Crystallogr. Chem.* **1982**, *38B*, 2134–2139.

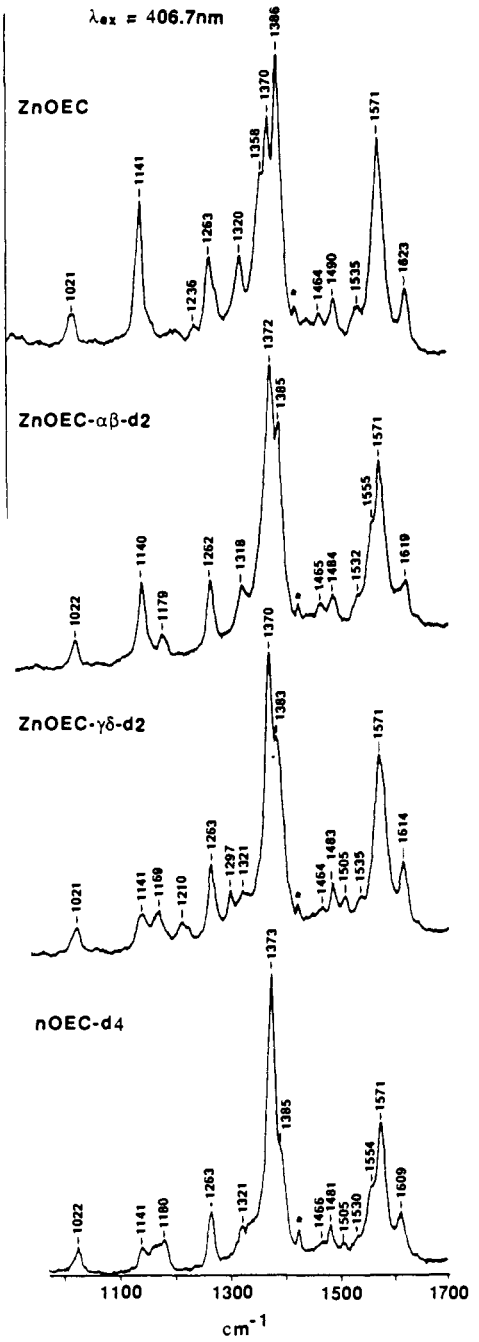

Figure 2. Resonance Raman spectra of ZnOEC, ZnOEC-α,β-d_2, ZnOEC-γ,δ-d_2, and ZnOEC-d_4 in CH_2Cl_2 solutions obtained with Soret excitation at 406.7 nm. Laser power, 7 mW; concentration, ~70 μM. The asterisk denotes a solvent band.

attempting any perturbative refinement of the force field. This procedure brought the calculated skeletal frequencies of CuOEC into better accord with those observed. This force field is designated FF I in Table II. Only those force constants that are different from those reported by Prendergast and Spiro[41] are listed in the table. For reference, the force field obtained by reversing the C_aC_m stretching force constants of FF I is also listed in the table and is designated FF II. For this force field and all others described below, only those force constants that are different from those of FF I are included in the table.

During the course of the vibrational analyses, a large number of strategies were employed in attempts to improve the fit between the observed and calculated vibrational frequencies and isotope shifts. These approaches were based on systematically varying selected diagonal and off-diagonal force constants of the ring skeleton. In all cases the force constants for the reduced ring, the ethyl groups, and the *meso*-hydrogens were held fixed. The force constants for two additional representative force fields that give reasonable fits to the data are also given in Table II. One of the force fields was obtained by first refining all of the

Table II. Force Constants for CuOEC

		on or adjacent to pyrrole ring			
	force const	I	II_1	II_2	III
FF I	κ(aN)	5.459	5.411	5.127	5.325
	κ(ab)	4.018	5.335	5.431	5.527
	κ(bb)	3.752	6.703		6.703
	κ(am)	6.819	6.390	6.819	6.390
	κ(MN)	1.443	1.571		1.499
FF II[a]	κ(am)	6.390	6.819	6.390	6.819
FF III[a]	κ(aN)	5.743	7.168	5.888	6.151
	κ(ab)	4.018	5.555	5.368	5.373
	κ(bb)	3.752	6.660		6.961
	κ(am)	5.138	6.964	6.776	6.470
	κ(MN)	1.503	1.636		1.561
	1,2 κ-κ(am-am)	0.2 ($I-II_1$)		0.4 (II_2-III)	
FF IV[a]	1,2 κ-κ(am-am)	0.435 ($I-II_1$)		0.412 (II_2-III)	
	1,4 κ-κ(am-am)	−0.362 (I-I)	−0.749 (II_1-II_2)		0.129 (III-III)

[a] All other force constants are the same as in force field I.

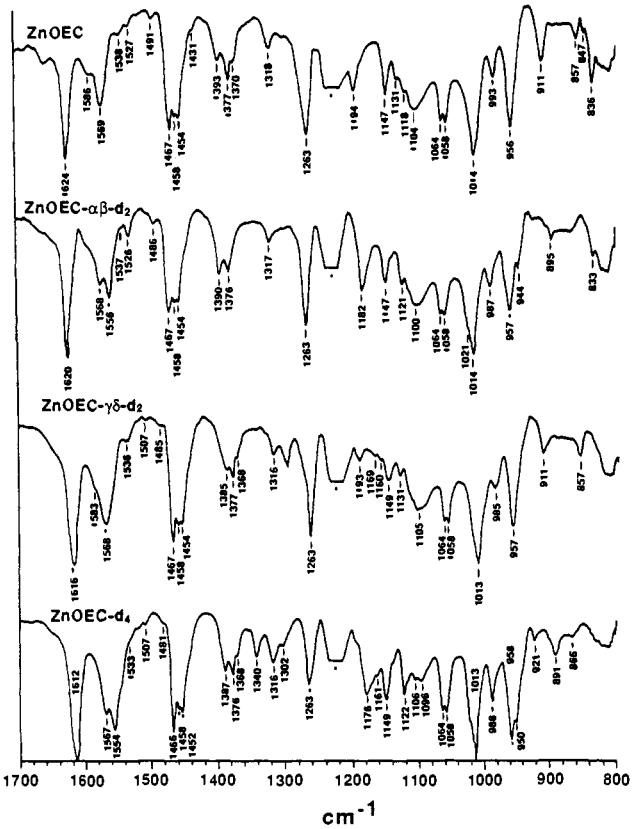

Figure 3. IR spectra of saturated $CHCl_3$ solutions of ZnOEC, ZnOEC-α,β-d_2, ZnOEC-γ,δ-d_2, and ZnOEC-d_4. The asterisk denotes a solvent band.

diagonal skeletal constants. This refinement was followed by a second iteration in which only the diagonal force constants of the C_aC_m and C_bC_b bonds were allowed to vary. Finally, the 1,2 C_aC_m–C_aC_m interaction constants for the α,β- and γ,δ-methine bridges were given different values because this improved the fit in the observed versus calculated *meso*-deuteriation shifts. This force field is designated FF III in Table II. The force field designated FF IV was obtained by adding 1,4 C_aC_m–C_aC_m interaction constants to FF I and then refining both these and the 1,2 C_aC_m–C_aC_m interaction constants.

Results

A. Vibrational Spectra of CuOEC and ZnOEC. Figure 2 shows the Soret-excitation resonance Raman spectra for ZnOEC, ZnOEC-α,β-d_2, ZnOEC-γ,δ-d_2, and ZnOEC-d_4 in CH_2Cl_2 solutions. The IR spectra for this set of ZnOEC complexes in $CHCl_3$ solutions are shown in Figure 3. The total number of bands observed in the IR spectra is greater than the number detected

Table III. Vibrational Frequencies (cm^{-1}), Isotope Shifts (cm^{-1}), and Symmetries for the High-Frequency Modes of CuOEC[a,b] and ZnOEC[b]

CuOEC				ZnOEC				
h_4	$\Delta\alpha,\beta$-d_2	$\Delta\gamma,\delta$-d_2	Δd_4	h_4	$\Delta\alpha,\beta$-d_2	$\Delta\gamma,\delta$-d_2	Δd_4	sym
1644	−3	−7	−10	1623	−4	−9	−14	A
1602	−12	−2	−13	1586	−18	−3	−19	A
1584	−10	−4	−11	1569	−13	−1	−15	B
1583	−1	−1	−1	1571	0	0	0	A
1547	−1	0	−3	1538	−1	−2	−5	A
1543	0	−17	−17	1527	−1	−20	−20	B
1507	−6	−6	−13	1490	−6	−7	−9	A
1486[c]	−4	−7	−10					A

[a] Reference 42. [b] This work. [c] Enhanced by visible excitation.

Table IV. Observed[a] and Calculated[b] Frequencies and Isotope Shifts (cm^{-1}) for the High-Frequency Skeletal Modes of CuOEC

obsd				$\Delta\alpha,\beta$-d_2		$\Delta\gamma,\delta$-d_2		Δ-d_4		$\Delta^{15}N$		
RR	IR	calcd	sym	obsd	calcd	obsd	calcd	obsd	calcd	obsd	calcd	assignment[d]
1644 (p)[c]	1644	1645	A	3	1	7	11	10	14	0	0	57% $\nu C_aC_m(\gamma,\delta)$, 10% $\delta C_mH(\gamma,\delta)$
		1618	B		5		7		15		0	36% $\nu C_aC_m(\gamma,\delta)$, 30% $\nu C_aC_m(\alpha,\beta)$
1602 (p)	1602	1616	A	12	11	2	5	13	14	1	0	52% $\nu C_aC_m(\alpha,\beta)$, 10% $\nu C_aC_m(\gamma,\delta)$, 10% $C_mH(\alpha,\beta)$
1584 (dp)	1583	1582	B	10	8	4	14	11	18	0	0	32% $\nu C_aC_m(\gamma,\delta)$, 32% $\nu C_aC_m(\alpha,\beta)$
1583 (p)		1571	A	1	3	1	0	1	3		0	27% νC_bC_b(III), 11% νC_bC_b(II,IV), 13% $\nu C_aC_m(\alpha,\beta)$
		1557	B		5		1		6		1	45% νC_bC_b(II,IV), 8% $\nu C_aC_m(\alpha,\beta)$, 4% $\nu C_aC_m(\gamma,\delta)$
1547 (p)	1547	1561	A	1	0	0	1	3	2	0	1	28% νC_bC_b(II,IV), 20% νC_bC_b(III), 6% $\nu C_aC_m(\alpha,\beta,\gamma,\delta)$
1543 (ap)	1543	1453	B	0	2	17	6	17	7		3	21% $\nu C_aC_m(\gamma,\delta)$, 9% $\nu C_aN(II_1,IV_1)$
1507 (p)	1507	1491	A	6	3	6	4	13	9	1	1	15% $\nu C_aC_m(\alpha,\beta)$, 15% $\nu C_aC_m(\gamma,\delta)$, 20% νC_bC_b(II,IV)
1486 (p)	1484	1470	A	4	5	7	7	10	10		2	21% $\nu C_aC_m(\gamma,\delta)$, 16% $\nu C_aC_m(\alpha,\beta)$, 12% νC_aN(II,IV)
1466 (dp)		1461	B		4		1		7		2	22% $\nu C_aC_m(\alpha,\beta)$, 10% νC_aN(III)
1403 (dp)		1392	B	0	4	4	0	7	3	1	1	32% νC_aC_b(III), 16% νC_bC_1
1388	1396	1385	B	2	5	5	0	4	5		1	26% νC_aC_b(II,IV), 16% νC_bC_1
1373 (p)	1375	1386	A	3	1	2	1	2	2	6	1	29% νC_aC_b(II,IV), 20% νC_bC_1
1362 (p)		1355	A		2		2		3	5	3	12% $\nu C_aN(II_2,IV_2$,III), 9% νC_aC_b(III)
1352 (p)		1343	A		3		2		5	4	3	17% $\nu C_aN(II_1,IV_1$,III), 6% νC_aC_b(III)
1318 (ap)	1318	1315	B	1	2	1	2	2	5	1	3	26% νC_aN(II,IV), 22% νC_aC_b(II,IV)
		1313	A		1		2		3		4	20% νC_aN(I,III), 9% νC_aC_b(III), 7% νC_aN(II,IV)
1307		1291	B	+10	+6		424		394	5	4	19% νC_aN(I), 18% $\delta C_mH(\gamma,\delta)$
		1305	B		198		0		197		1	8% $\delta C_mH(\alpha,\beta)$, 37% CH_2 twist
		1296	A		0		7		7		2	14% νC_aN(I), 20% CH_2 twist
1277 (ap)		1259	B	+11	0	+16	+17	+27	+16		2	13% νC_aN(I), 13% $\nu C_aC_b(II_1,IV_1)$
1275 (p)		1286	A	99	127	2	0	97	122		0	7% $\delta C_mH(\alpha,\beta)$, 52% CH_2 twist
		1258	A		1		1		3		8	22% νC_aN(I), 15% νC_bC_b(I)
1238 (p)		1218	A	292	308	14	1	292	263		+6	30% $\delta C_mH(\alpha,\beta)$, 20% $\nu C_aC_b(II_2,IV_2$,III)
1215 (ap)	1211	1218	B		353	0	0		366		1	27% $\delta C_mH(\alpha,\beta)$, 17% νC_aC_b(III)
1198 (p)	1197	1210	A	0	+2		289		263	0	3	35% $\delta C_mH(\gamma,\delta)$, 18% $\nu C_aC_b(I,II_1,IV_1)$
1155 (dp)		1130	B		0	0	+9		+9	10	6	24% νC_aN(III), 22% νC_bC_1
1141 (p)		1118	A	0	0	+32	+24	+32	+21	13	9	23% $\nu C_aN(II_1,IV_1)$, 18% νC_bC_1
1129 (ap)	1128	1147	B	6	1	0	22	6	22	19	5	19% νC_aC_b(I), 13% νC_aN(I), 10% $\delta C_mH(\gamma,\delta)$
		1108	A		+176		0		+173		9	20% $\nu C_aN(II_2,IV_2)$, 14% $\delta C_mH(\alpha,\beta)$
		1117	B		2		+114		+114		6	12% $\nu C_aN(II_1,IV_1)$, 12% νC_bC_1
		1108	B		+68		0		+75		3	17% $\nu C_aN(II_2,IV_2)$, 12% νC_bC_1
		1104	B		+182		+2		+189		8	24% νC_bC_1
		1092	A		+6		+10		+14		4	10% νC_aC_b(III), 8% $\delta C_mH(\alpha,\beta)$, 8% $\delta C_mH(\gamma,\delta)$
		1088	B		+8		+10		+11		5	20% $\delta C_mH(\alpha,\beta,\gamma,\delta)$, 10% C_aN(I,II,IV)
		1060	A		0		+7		+6		7	15% νC_aC_b(I,III), 11% νC_1C_2
		1035	A		0		0		0		2	20% δC_aC_bH(I), 16% νC_aC_b(I)

[a] The RR and IR frequencies for CuOEC and the *meso*-deuteriated isotopomers were taken from ref 42. The ^{15}N shifts are from ref 31. [b] Calculated with FF I (see text). [c] Abbrevations: p, polarized; ap, anomalously polarized; dp, depolarized. [d] Mode descriptions are as follows: ν = stretch and δ = in-plane deformation. C_a, C_b, C_m, and the characters in parentheses refer to the macrocyclic positions shown in Figure 1.

in the resonance Raman spectra owing to the IR activity of the internal vibrations of the ethyl groups. Soret-excitation resonance Raman spectra of CuOEC, CuOEC-α,β-d_2, CuOEC-γ,δ-d_2, and CuOEC-d_4 in CH_2Cl_2 solutions are shown in Figure 4. These spectra complement the visible-excitation resonance Raman spectra obtained in our earlier work.[42,62]

Comparison of the vibrational data for ZnOEC (Figures 2 and 3) with those for CuOEC (Figure 4 and our earlier work[42]) shows a close correspondence in the bands observed and in the pattern of vibrational frequency shifts upon selective *meso*-deuteriation. These data for selected modes of CuOEC and ZnOEC are compared in Table III. A detailed discussion of the mode assignments will be presented below. Here, we make some general observations and comment on the characteristics of several modes in the high-frequency region.

The metal-dependent frequency differences between the modes correlated in Table III arise from the larger core size, and correspondingly lower macrocycle mode frequencies, for ZnOEC relative to CuOEC. These metal dependencies have been observed for metallochlorins by several authors[31,32,42] and correspond to the well-known core-size dependence of metalloporphyrin macrocycle modes.[63] In our original work on CuOEC, the IR and visible-excitation resonance Raman data showed two prominent bands in the 1580–1605-cm^{-1} region. The ZnOEC data presented here and the normal coordinate calculations discussed below indicate that a third band should be apparent in this frequency region (for ZnOEC, the corresponding frequency region is 1565–1590 cm^{-1}

(62) Because of its longer singlet lifetime and higher fluorescence yield, we have not been able to record visible excitation RR spectra for ZnOEC and its selectively *meso*-deuteriated compounds.

(63) Spaulding, L. D.; Chang, C. C.; Yu, N.-T.; Felton, R. H. *J. Am. Chem. Soc.* **1975**, *97*, 2517–2524.

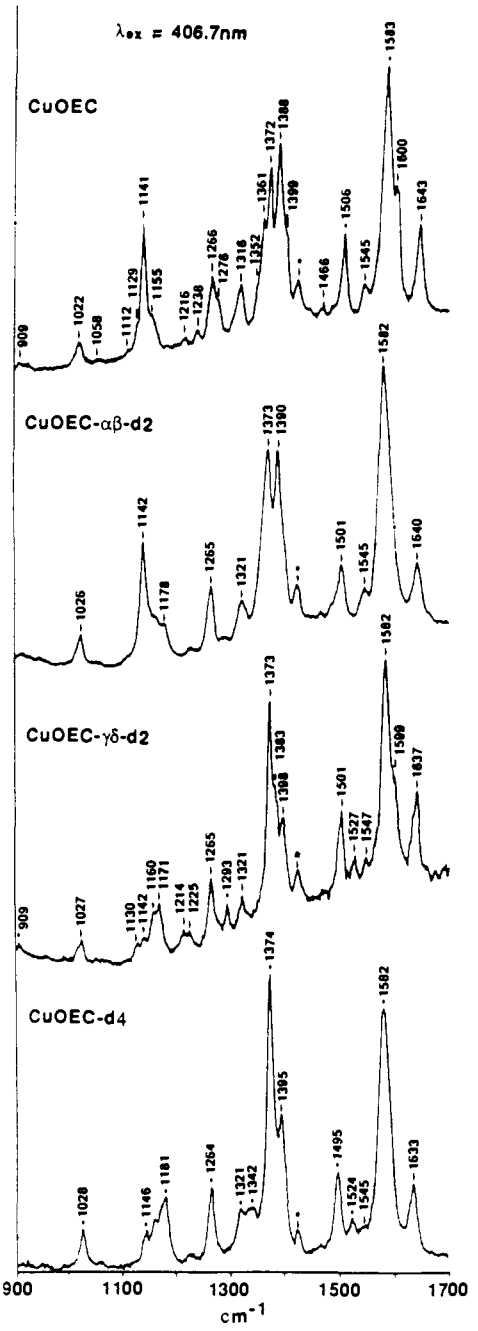

Figure 4. Resonance Raman spectra of CuOEC, CuOEC-α,β-d_2, CuOEC-γ,δ-d_2, and CuOEC-d_4 in CH_2Cl_2 solution obtained with Soret excitation at 406.7 nm. Laser power, 7 mW; concentration, ~40 μM. The asterisk denotes a solvent band.

and the three modes occur at 1569, 1571, and 1586 cm^{-1} in the *meso*-h_4 species (Table III)). Accordingly, we obtained higher resolution IR spectra of CuOEC and its specifically *meso*-deuteriated derivatives (not shown). These spectra revealed the presence of a third band at 1583 cm^{-1} (Table III). Inspection of the IR (figure 3) and polarized resonance Raman (not shown) spectra of ZnOEC also revealed that the 1535-cm^{-1} band observed in the Soret-excitation resonance Raman spectrum (Figure 2) is due to two overlapping bands, one at 1538 cm^{-1} (polarized) and the other at 1527 cm^{-1} (anomalously polarized). The properties and frequency shift patterns of these modes correspond closely to those of the 1547- (polarized) and 1543-cm^{-1} (anomalously polarized) bands of CuOEC.

The compilation of mode frequencies and *meso*-deuteriation shifts for CuOEC and ZnOEC in Table III shows that the frequency shift pattern observed for CuOEC upon selective *meso*-deuteriation parallels that observed for ZnOEC. The magnitudes

Table V. Comparison of the Frequencies and Deuteriation Shifts (cm^{-1}) for the Various Force Fields

		$\Delta\alpha,\beta$-d_2	$\Delta\gamma,\delta$-d_2	Δ-d_4
obsd	1644	3	7	10
FF I	1645	1	11	14
FF II	1640	2	8	14
FF III	1646	3	7	13
FF IV	1642	7	6	15
FF V	1647	1	12	15
FF VI	1648	0	10	10
FF VII	1649	0	11	11
obsd	1602	12	2	13
FF I	1616	11	5	14
FF II	1617	10	8	15
FF III	1613	8	6	12
FF IV	1604	6	12	15
FF V	1615	11	5	15
FF VI	1618	10	0	10
FF VII	1624	8	0	8
obsd	1584	10	4	11
FF I	1582	8	14	18
FF II	1578	15	6	18
FF III	1590	12	4	14
FF IV	1581	13	7	18
FF V	1581	8	14	21
FF VI	1607	10	1	10
FF VII	1613	9	2	10
obsd	1583	2	1	1
FF I	1571	3	0	3
FF II	1576	3	1	3
FF III	1590	3	0	3
FF IV	1572	2	0	2
FF V	1573	8	2	9
FF VI	1562	2	1	4
FF VII	1589	3	1	4
obsd	1547	1	0	3
FF I	1561	0	1	2
FF II	1561	0	2	2
FF III	1556	1	2	4
FF IV	1552	0	1	1
FF V	1544	1	3	4
FF VI	1533	4	2	5
FF VII	1561	3	1	4
obsd	1543	0	17	17
FF I	1453	2	6	7
FF II	1450	0	24	25
FF III	1474	4	18	21
FF IV	1466	2	6	10
FF V	1466	1	10	10
FF VI	1507	6	2	8
FF VII	1504	3	3	7
obsd	1507	6	6	13
FF I	1491	3	4	9
FF II	1492	1	6	8
FF III	1511	3	6	12
FF IV	1494	6	4	11
FF V	1485	6	6	6
FF VI	1481	3	5	8
FF VII	1488	3	5	8
obsd	1486	4	7	10
FF I	1470	5	7	10
FF II	1469	7	5	10
FF III	1486	7	11	16
FF IV	1474	3	7	10
FF V	1493	3	5	12
FF VI	1491	3	0	4
FF VII	1409	6	13	20
obsd	1403	0	4	7
FF I	1392	4	0	3
FF II	1392	3	0	3
FF III	1401	7	2	7
FF IV	1392	4	0	4
FF V	1371	5	0	5
FF VI	1490	1	5	6
FF VII	1457	3	2	4

Table VI. Average Errors between the Observed and Calculated Frequencies and Deuteriation Shifts for Various Force Fields[a]

FF	Δ, cm^{-1}	$\Delta\Delta d$, cm^{-1}	description
I	13.5 (8.40)	2.89 (2.47)	force field for NiOEC with scaled diagonal force constants
II	14.2 (9.00)	2.43 (2.20)	same as I with C_aC_m force constants reversed
III	11.6 (7.73)	2.48 (2.43)	skeletal diagonal force constants refined, 1,2 C_aC_m–C_aC_m interaction constants adjusted
IV	12.1 (7.86)	2.69 (2.35)	same as I but only 1,3 C_aC_m–C_aC_m and 1,4 C_aC_m–C_aC_m interaction constants refined
V	20.6 (16.8)	4.51 (4.47)	same as I but with QCFF/PI optimized geometry
VI	29.7 (29.3)	4.72 (3.83)	QCFF/PI point masses
VII	34.1 (33.8)	3.94 (3.50)	QCFF/PI ethyl groups

[a] Values tabulated from the 16 observed bands and 37 observed deuteriation shifts in the 1650–1300-cm^{-1} region. [b] Values in parentheses do not include the observed 1543-cm^{-1} band and its corresponding deuteriation shifts.

Table VII. s^2 Values between Various Force Fields ($\times 10^{-3}$)

	I	II	III	IV	V	VI	VII
I		0.2	2.1	0.4	2.7	26 (13)[a]	30
II	0.2		1.7	0.59	2.9	27	30
III	2.1	1.7		2.5	4.9	29	33
IV	0.4	0.59	2.5		3.1	26	30
V	2.7	2.9	4.9	3.1		23	27
VI	26 (13)[a]	27	29	26	23		2.2
VII	30	30	33	30	27	2.2	

[a] s^2 calculated with 1,4 and higher interactions excluded.

of the shifts observed for ZnOEC are greater than those observed for CuOEC owing to the lower C_aC_m frequencies and hence better fixing with the C_mH deformations. Regardless, a number of the corresponding modes of the two different MOEC complexes exhibit α,β-deuteriation shifts that are distinct from those observed upon γ,δ-deuteriation. These data confirm that the mode localization phenomenon in MOEC complexes does not depend on the central metal ion but rather on the symmetry of the macrocycle, as has been previously suggested.[37,42]

B. Vibrational Assignments and Force Field Comparisons for MOEC Complexes. The vibrational assignments for the high-frequency (above 1000 cm^{-1}) skeletal modes of CuOEC are given in Table IV. These assignments were made on the basis of the frequencies, isotope shifts, and RR band polarizations of the various modes. The calculated frequencies and potential energy distributions listed in the table were obtained with FF I. Table V compares the frequencies and *meso*-deuteriation shifts for nine high-frequency skeletal modes calculated by using this force field with those predicted by the other three empirical force fields. Frequency and *meso*-deuteriation shift data from three additional calculations are also listed in Table V. FF V is a calculation performed with the **F** matrix for FF I and a **G** matrix constructed from the QCFF/PI optimized geometry. This calculation was performed because the semiempirical calculation produces an energy-minimized geometry that differs from that used in the empirical calculation (see Table I). FF VI and FF VII are QCFF/PI calculations in which the ethyl groups are treated either as point masses or explicitly, respectively.

The average errors between the observed and calculated frequencies and *meso*-deuteriation shifts are compared for all seven force fields in Table VI. These errors were determined on the basis of the 16 highest frequency observed RR bands and 37 *meso*-deuteriation shifts. These bands correspond to C_aC_m, C_bC_b, C_aN, and C_aC_b stretching motions. The seven force fields were also compared with each other by using the method described by Strauss and co-workers.[64] In this approach, the mass-weighted Cartesian **F** matrix is computed for each force field. The use of the Cartesian **F** matrices allows direct comparison of the empirical force fields with those calculated by using the QCFF/PI method. The degree of similarity between two force fields is then given by the similarity factor s^2 calculated according to eq 1. Here

$$s^2 = 1/(3N-6)\sum_{i=1}^{3n}\sum_{j=1}^{3n}(\mathbf{F}^1_{ij} - \mathbf{F}^2_{ij})^2 \qquad (1)$$

$\mathbf{F}^1$ and $\mathbf{F}^2$ are the mass-weighted cartesian coordinate **F** matrices for the two force fields and N corresponds to the number of atoms. The s^2 values for the seven different force fields are given in Table VII. These values were calculated by using only the **F** matrix elements of the atoms in the ring skeleton (including the *meso*-hydrogens). The **F** matrix elements of the ethyl group atoms and reduced-ring hydrogens were excluded from the calculations because their positions in the QCFF/PI optimized geometry are quite different from those used in the empirical calculations. These geometry differences result in large constributions to the computed s^2 values that obscure the contributions due to differences in the skeletal portions of the force fields.

Discussion

A. Vibrational Assignments. The selective *meso*-deuteriation data in conjunction with the normal coordinate calculations permit us to refine our previous interpretation of the vibrational spectra of CuOEC. These refinements are readily extended to the spectra of other MOEC complexes as the compilation in Table III indicates. Most of the modes above 1000 cm^{-1} can now be assigned with a reasonable degree of confidence. Many of the vibrational assignments reported in Table III are consistent with previous qualitative interpretations of the spectra of CuOEC.[31,42] However, the new information reported herein necessitates the reevaluation of certain assignments. The specific assignments for selected high-frequency skeletal modes are discussed in more detail below.

1. C_aC_m Vibrations. There are eight C_aC_m vibrations expected in the high-frequency region (4 A and 4 B). Inspection of Table III reveals that seven of the eight modes are observed in the vibrational spectra (1644, 1602, 1584, 1543, 1507, 1486, and 1466 cm^{-1}). The only missing vibration is the highest frequency B-symmetry mode which is calculated at 1618 cm^{-1}. In our study of NiOEC,[37] a band was observed near 1644 cm^{-1} that could be the analog of the missing C_aC_m mode of CuOEC. If so, the corresponding RR band of CuOEC would be expected at slightly lower frequency. In a previous RR study of CuOEC, Ozaki et al. assigned the 1602-cm^{-1} band to a totally symmetric C_bC_b stretching motion.[31] However, the *meso*-deuteriation data indicate that this band is associated with a C_aC_m mode localized on the α,β-methine bridges.[42] One other C_aC_m vibration that is worthy of note is the mode observed at 1543 cm^{-1} in both the IR and RR spectra. This band is assigned as a B-symmetry, γ,δ-methine-bridge localized C_aC_m vibration on the basis of its RR polarization (anomalous) and *meso*-deuteriation shift pattern (0 cm^{-1} in CuOEC-α,β-d_2; 17 cm^{-1} in both CuOEC-γ,δ-d_2 and CuOEC-d_4; 1 cm^{-1} in ZnOEC-α,β-d_2; 20 cm^{-1} in both ZnOEC-γ,δ-d_2 and ZnOEC-d_4). The frequency of this band is anomalously high and not reproduced in any force field calculations (Tables IV and V). Nevertheless, the significant intensity and large *meso*-deuteriation shifts of this band leave no recourse but to attribute it to a C_aC_m fundamental vibration.

(64) Bradley, G. M.; Siddall, W.; Strauss, H. L.; Varetti, E. L. *J. Phys. Chem.* **1975**, *79*, 1949–1953.

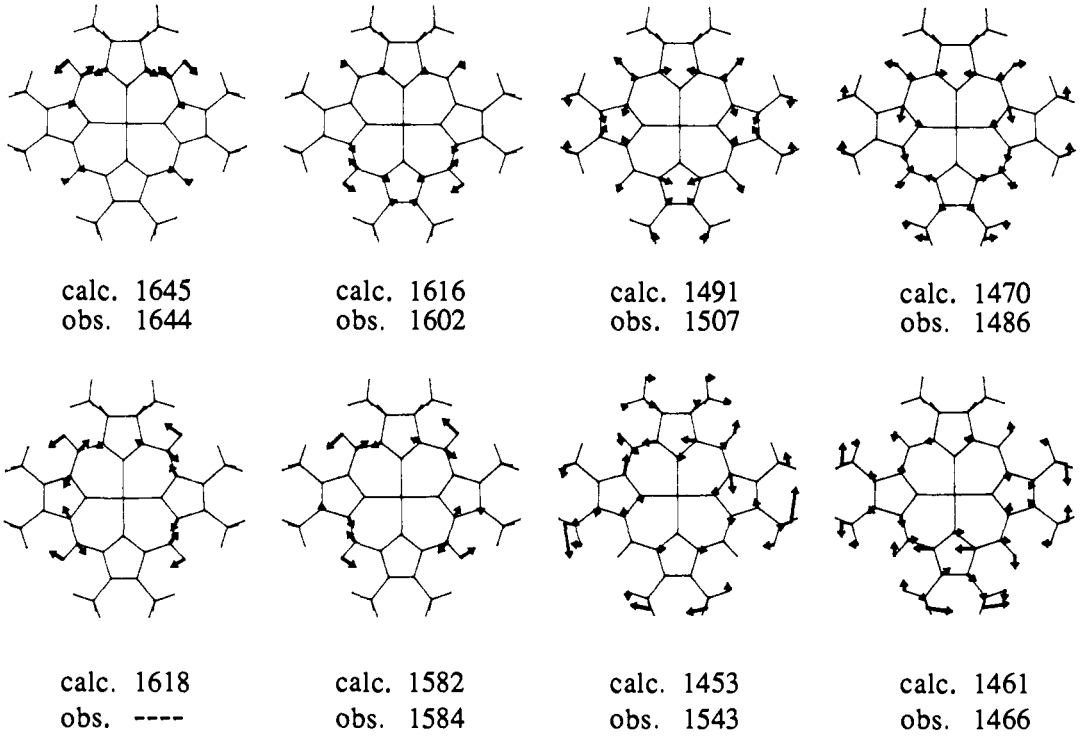

Figure 5. Vibrational eigenvectors of CuOEC which contain substantial contributions from C_aC_m stretching motions. Displacements are shown only for those atoms whose motions contribute significantly to the normal mode (10% or greater of the maximum atomic displacement of a given mode).

2. C_bC_b Vibrations. There are three C_bC_b vibrations expected in the high-frequency region (2 A and 1 B). The fourth C_bC_b stretch is associated with the reduced ring and expected at lower frequency. Of the three high-frequency C_bC_b vibrations, the two A-symmetry modes are observed in the vibrational spectra (1583 and 1547 cm^{-1}). The B-symmetry band is not observed but is calculated at 1557 cm^{-1} (FF I). In NiOEC, the analog of the B-symmetry band is observed at 1572 cm^{-1}.[37,41,42] Accordingly, the B-symmetry vibration of CuOEC would most likely fall in the 1560–1570-cm^{-1} region.

3. C_aC_b and C_aN Vibrations. There are eight C_aN and six C_aC_b modes expected in the high-frequency region (4 A and 4 B; 3 A and 3 B). Two other C_aC_b modes are associated with the reduced ring and expected at lower frequency. The C_aC_b and C_aN vibrations are extensively mixed with one another and with other motions of the macrocycle (Table III). Consequently, it is not generally appropriate to classify the observed bands as a specific type of mode. Inspection of the vibrational data for CuOEC reveals that there are eight prominent bands that can be associated with C_aC_b and C_aN vibrations (1403, 1388, 1373, 1362, 1318, 1155, 1141, and 1129 cm^{-1}). All of these bands have analogs in the spectra of NiOEC and most have been identified on the basis of their ^{15}N shifts.[31]

4. C_mH Vibrations. There are four C_mH deformations (2 A and 2 B). These modes are extensively mixed with other vibrations of the macrocycle as is evidenced by the complicated *meso*-deuteriation shift patterns observed in the 1100–1300-cm^{-1} region. On the basis of the spectral data for CuOEC and the normal coordinate calculations, we have assigned the bands at 1307, 1238, 1215, and 1198 cm^{-1} as the four C_mH deformations. All of these bands have analogs in the spectra of NiOEC;[31,37,41,42] however, in our previous assignments for this complex only the 1307-cm^{-1} band was attributed to a C_mH deformation.[37] Furthermore, we originally attributed this band to a mode localized on the α,β-methine bridges. The revised assignment and normal coordinate calculations presented here indicate that the motion is actually localized on the γ,δ-methine bridges.

The specific assignments for the C_mH deformations are worthy of additional comment. These assignments were derived in the following manner: In the case of the B-symmetry 1307-cm^{-1} band, a large *meso*-deuteriation shift is observed in CuOEC-γ,δ-d_2 and CuOEC-d_4. This is not immediately apparent because the spectra of both of these isotopomers exhibit an anomalously polarized band in the 1320–1325-cm^{-1} region.[42] However, this latter band is actually the analog of a band observed at 1318 cm^{-1} in the normal isotopomer. In CuOEC, this band is very weak, but its intensity increases in CuOEC-γ,δ-d_2 and CuOEC-d_4. The fact that the 1318-cm^{-1} band is a different mode, not associated with a C_mH deformation, is clearly revealed in both the IR and RR spectra of CuOEC-d_4 which exhibit a strong band in this region. Our original assignment of the 1308-cm^{-1} band of NiOEC as a α,β-methine-bridge localized C_mH deformation was based on misidentification of a band near 1314 cm^{-1} in NiOEC-γ,δ-d_2 as the upshifted analog of the 1308-cm^{-1} band rather than a different mode.[37] It should also be noted that the apparent absence of the 1307-cm^{-1} band in the spectrum of CuOEC-α,β-d_2 is due to the fact that this mode upshifts approximately 10 cm^{-1} in this isotopomer and becomes a shoulder on the low-energy side of the 1318-cm^{-1} band. This upshift is predicted by the normal coordinate calculations (Table IV). The band associated with the A-symmetry analog of the 1307-cm^{-1} vibration is more difficult to identify. We have attributed the 1198-cm^{-1} band to this mode on the basis of its selective shifts in the spectra of CuOEC-γ,δ-d_2 and CuOEC-d_4. The assignment of the 1238- and 1215-cm^{-1} bands as the A- and B-symmetry C_mH deformations localized on the α,β-methine bridges was also based on the selective *meso*-deuteriation shifts of these bands. Neither of these modes is significantly perturbed in the spectra of CuOEC-γ,δ-d_2, but both are significantly shifted in the spectra of CuOEC-α,β-d_2 and CuOEC-d_4.[42]

In addition to the four bands discussed above, several other modes are quite sensitive to *meso*-deuteriation. In particular, the 1275-cm^{-1} band appears to be comprised of two *meso*-deuteriation-sensitive bands (one polarized and the other anomalously polarized). In the CuOEC-α,β-d_2, the anomalously polarized band upshifts to 1288 cm^{-1}, while the polarized band downshifts to 1178 cm^{-1}. This reveals a band at 1263 cm^{-1} which is attributable to a CH_2 deformation of the ethyl groups.[59] In CuOEC-γ,δ-d_2, the anomalously polarized band upshifts to approximately 1293 cm^{-1}, while the polarized band does not shift. Deuteriation sensitivity is also observed for the 1141-cm^{-1} band. In CuOEC-α,β-d_2 this mode does not shift, whereas in CuOEC-γ,δ-d_2 the band upshifts

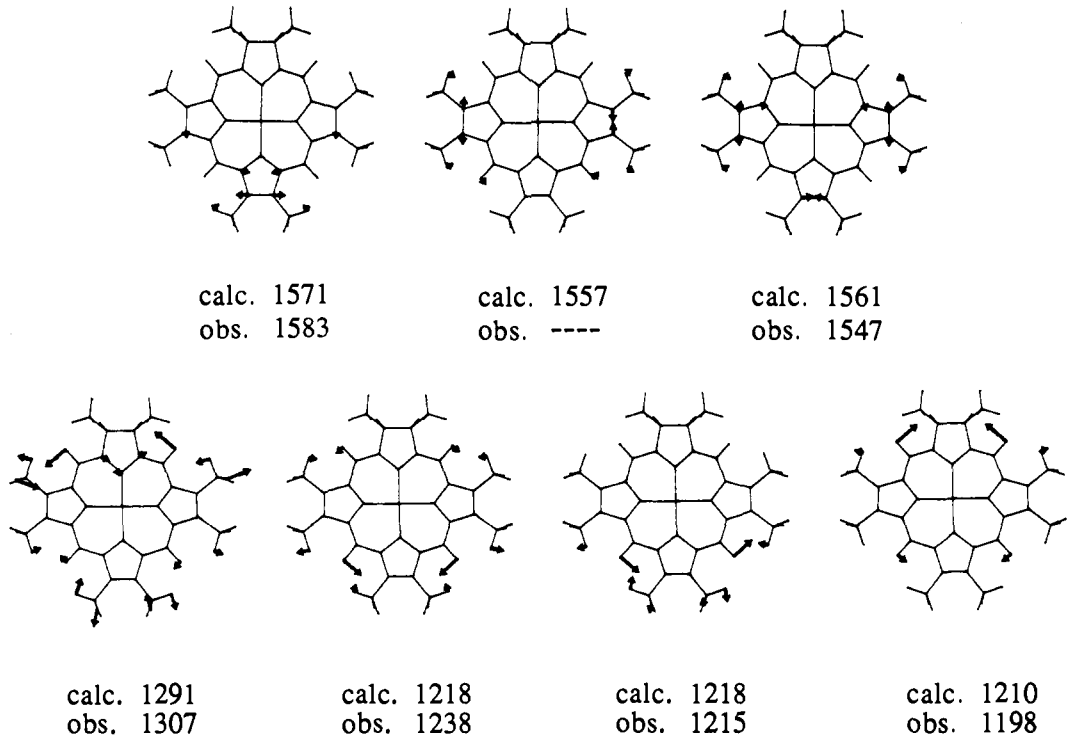

Figure 6. Vibrational eigenvectors of CuOEC which contain substantial contributions from C_bC_b stretching motions (top row) and C_mH deformations (bottom row). Displacements are shown only for those atoms whose motions contribute significantly to the normal mode (10% or greater of the maximum atomic displacement of a given mode).

to 1173 cm^{-1}. In CuOEC-d_4, the 1141-cm^{-1} band upshifts to 1180 cm^{-1}. This band falls at nearly the same frequency as the 1178-cm^{-1} band of CuOEC-γ,δ-d_2 (1275 cm^{-1} of the normal isotopomer). Consequently, the 1178-cm^{-1} band of CuOEC-d_4 is probably a superposition of the upshifted 1141-cm^{-1} and downshifted 1275-cm^{-1} bands.

B. Comparison of the Force Fields. 1. General Features of the Calculations. The objectives of our empirical calculations on CuOEC were to develop a satisfactory force field for MOEC complexes and determine the factors that influence the vibrational eigenvectors. In addition, we wanted to compare the forms of the eigenvectors obtained from the empirical calculation with those obtained by the QCFF/PI method. As was previously noted, our semiempirical calculations on MOEC complexes predict that the normal modes of the metallochlorins are different from those of metalloporphyrins.[37] In particular, the QCFF/PI method predicts that the vibrational eigenvectors of a number of the skeletal modes are localized on sectors of the macrocycle. The localization is most pronounced in the vibrations involving the methine bridges. This localization phenomenon was attributed to the length alteration pattern that occurs in the C_aC_m bonds of the OEC macrocycle.[58,60,61] Indeed, the vibrational data obtained for selectively *meso*-deuteriated CuOEC and ZnOEC support the idea of localized eigenvectors for certain modes.[42]

Although the semiempirical calculations and the general observations of the selective *meso*-deuteriation studies strongly suggest that some degree of eigenvector localization occurs in MOEC complexes, the empirical calculations on NiOEC by Prendergast and Spiro predict that the vibrational eigenvectors of this complex are delocalized and are generally similar to those of NiOEP.[41] This latter prediction prompted us to carefully examine the vibrational eigenvectors obtained in the course of our empirical calculations on CuOEC. In all cases, our calculations predict certain vibrational eigenvectors are localized. The localization phenomenon is manifested regardless of whether the force field gives a reasonable fit to the vibrational data. The localization is particularly apparent in modes associated with the C_aC_m stretches and C_mH deformations. This is illustrated in Figures 5–7 which depict selected vibrational eigenvectors for CuOEC. These eigenvectors were calculated by using FF I. The prediction of localized modes in all of our empirical calculations leads us to conclude that mode localization is a general consequence of symmetry lowering and does not depend on the fine details of the force field or the molecular structure. This conclusion is further supported by the observation that the isotope-shift patterns observed for selectively *meso*-deuteriated ZnOEC are virtually identical with those observed for CuOEC. Finally, it should be noted that Li and Zgierski recently reported detailed normal coordinate calculations for free base and nickel(II) porphine.[65] These workers predict that the free base has a number of localized vibrational modes. This localization occurs as a consequence of the bond-length disparities that occur in the low symmetry free base. The localization is apparent in the eigenvectors of free base porphine despite the fact that the bond length disparities[66] are significantly smaller than those in MOEC complexes.[58,60,61]

2. Relative Merits of Individual Force Fields. Inspection of Table VI reveals that FF I–FF IV are approximately comparable in their quality as judged by the calculated average errors in the frequencies and *meso*-deuteriation shifts. The errors calculated with FF V (empirical calculation with QCFF/PI optimized geometry) are somewhat larger. As expected, the average errors in the frequencies obtained by the QCFF/PI method (FF VI and FF VII) are larger than those of any of the empirical calculations. However, the average errors in the *meso*-deuteriation shifts for the semiempirical force field are not substantially different from those of the empirical calculations. Regardless of the quality of the fits based on these criteria, none of the force fields adequately reproduce all of the detailed spectral features. For example, all of the empirical force fields significantly underestimate the frequency of the 1543-cm^{-1} C_aC_m vibration. This mode alone accounts for approximately 30% of the average error in the frequencies (Table V). Interestingly, the frequency of this mode is better reproduced in the QCFF/PI calculations. This result suggests that higher order interactions, not accounted for in the valence force fields, are important in determining the detailed vibrational characteristics of the OEC macrocycle.

(65) Li, X.-Y.; Zgierski, M. Z. *J. Phys. Chem.* **1991**, *95*, 4268–4281.
(66) Cullen, D. L.; Meyer, E. F. *J. Am. Chem. Soc.* **1974**, *96*, 2095–2102.

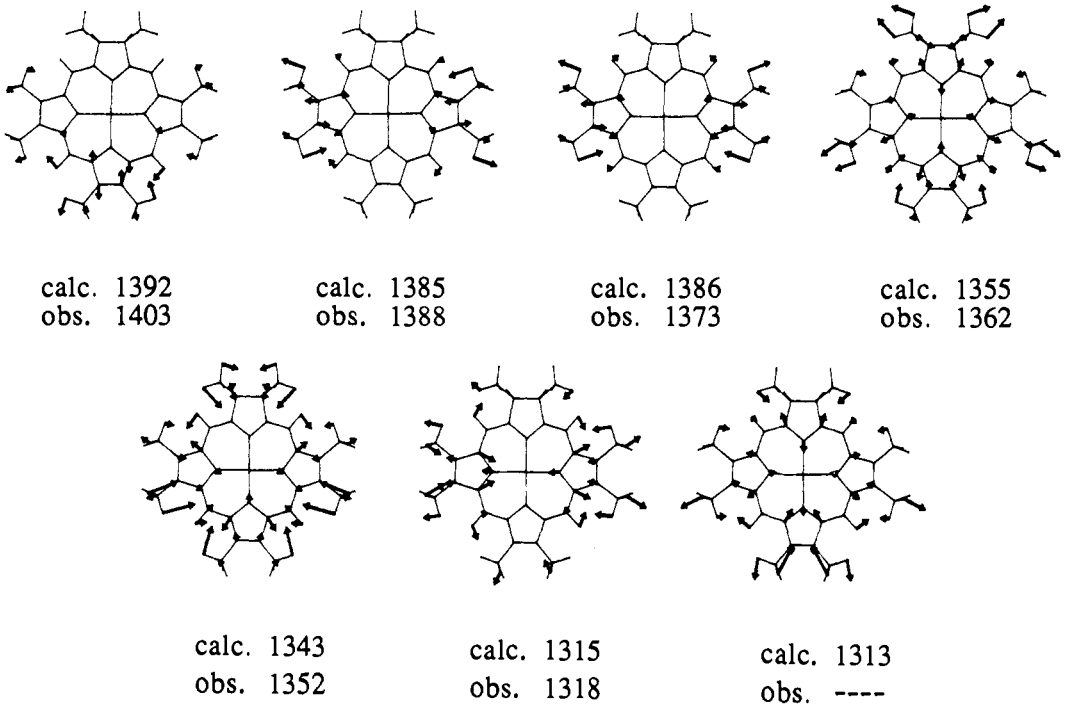

Figure 7. Vibrational eigenvectors of CuOEC which contain substantial contributions from both C_aC_b and C_aN stretching vibrations. Displacements are shown only for those atoms whose motions contribute significantly to the normal mode (10% or greater of the maximum atomic displacement of a given mode).

Inspection of Table V reveals that none of the empirical force fields accurately reproduce the selective *meso*-deuteriation shifts of all the skeletal modes. For example, the mode observed at 1602 cm^{-1} downshifts 12 cm^{-1} upon α,β-methine deuteriation, but only 2 cm^{-1} upon γ,δ-methine deuteriation. FF I predicts shifts of 11 and 5 cm^{-1}, respectively, which is a reasonable representation of the observed shift pattern. In contrast, FF II predicts shifts of 10 and 8 cm^{-1}; FF III predicts shifts of 8 and 6 cm^{-1}; and FF IV predicts shifts of 6 and 12 cm^{-1}. These predicted shift patterns are considerably less satisfactory than those obtained with FF I. On the other hand, FF I fails to predict the shift pattern observed for the 1584-cm^{-1} band, whereas the other three force fields give a satisfactory representation of the observed pattern. Specifically, the 1584-cm^{-1} band downshifts 10 cm^{-1} upon α,β-methine deuteriation and 4 cm^{-1} upon γ,δ-methine deuteriation. FF I predicts shifts of 8 and 14 cm^{-1}, respectively. FF II predicts shifts of 15 and 6 cm^{-1}; FF III predicts shifts of 12 and 4 cm^{-1}; and FF IV predicts shifts of 13 and 7 cm^{-1}. In the case of the 1543-cm^{-1} band, both FF I and FF IV fail to predict that large shifts are observed in CuOEC-γ,δ-d_2 and CuOEC-d_4. In contrast, both FF II and FF III do give a satisfactory representation of the observed shift pattern. Finally, it is interesting to note that the QCFF/PI calculations (FF VI and FF VII) accurately predict the *meso*-shift patterns of both the 1602- and 1584-cm^{-1} bands. Indeed, the semiempirical calculations satisfatorily reproduce the shift patterns for most of the high-frequency skeletal modes, with the exception of the 1543-cm^{-1} band. The miscalculation of the *meso*-deuteriation shifts of this mode is primarily responsible for the larger average errors obtained for the semiempirical versus the empirical calculations (Table VI).

On the basis of the above discussion, we conclude that both the empirical and semiempirical calculations give a reasonable accounting of the vibrational characteristics of MOEC complexes. The empirical force fields better reproduce the observed frequencies; however, this parameter is only one criterion for the assessment of the quality of a force field. Indeed, this criterion cannot be considered reliable if the isotope shifts are not also accurately reproduced. On the basis of the latter criterion, the semiempirical calculations are reasonable. Another criterion that has been used in deriving a satisfactory force field is the requirement that the force constants scale with the bond lengths.[41,59] In our calculations, this requirement is met by FF I and FF IV. In contrast, the force constants used for the C_aC_m bonds in FF II are in reverse order from those that should be used based on the bond lengths. In the case of FF III, the refinement increases the $Ca(II_1)$–N(II) stretching force constant from 5.411 to 7.168 mdyn/Å. Simultaneously, the C_aC_m force constant for the bond adjacent to ring I is reduced from 6.189 to 5.138 mdyn/Å. Both of these refined values are unreasonable on the basis of the lengths of the C_aC_m and C_aN bonds in tetrapyrrolic macrocycles.[67] Regardless, both FF II and FF III give reasonable average errors in both the frequencies and *meso*-deuteriation shifts. Indeed, by these criteria, FF III is the "best". This might be expected given that the force field was refined by using these criteria. Accordingly, the bond-length criterion, while appealing, is not necessarily a satisfactory indicator of the merit of a force field.

The apparent equivalency in merit of the various force fields led us to examine the s^2 factors between the individual force fields (Table VII). The s^2 values between the different empirical force fields are relatively small and similar to one another. Regardless, the calculated *meso*-deuteriation shift patterns for certain skeletal modes are quite different (vide supra). The s^2 values between the empirical and semiempirical force fields are much larger. Only a small part of this difference is due to the different geometries used in the two calculations (cf. FF V versus FF I and FF V versus FF VI). This result indicates that the large s^2 value between the empirical and semiempirical calculations lies in the partitioning of the force constants between the various internal coordinates. A significantly different partition might be expected between the two types of force fields because the **F** matrix used by the QCFF/PI calculation contains long-range interaction constants that are not included in the empirical force field. The inclusion of these off-diagonal interactions must necessarily affect the values of the diagonal force constants. In order to explore the contribution of higher order interaction constants to the s^2 values, all 1,4 and higher interaction constants were removed from the QCFF/PI **F** matrix and s^2 was recalculated between FF I and FF IV. This reduced the s^2 value by approximately 50% (from 0.025 to 0.013, see Table VI). This result indicates that 1,4 and

(67) Scheidt, W. R. In *The Porphyrins*; Dolphin, D., Ed.; Academic Press: New York, 1978; Vol. III, pp 463–512.

higher order interaction constants are the predominant factor contributing to the disparity in the empirical and semiempirical F matrices. Presuming that the higher order interactions are as important as suggested by the QCFF/PI calculation, force constants reflecting such interactions should also be included in empirical calculations. In this regard, Li and Zgierski found that the inclusion of certain 1,4 interaction constants was important in obtaining an accurate force field for porphines.[65] In our calculations on CuOEC, the effects of 1,4 interactions were explored only in a limited fashion. A detailed assessment of the effects of these (and higher order) interactions is not possible because there are a large number of these types of interactions and the experimental information is too limited to allow an evaluation of their importance.

Summary and Conclusions

The empirical force-field calculations reported herein indicate that various force fields satisfactorily reproduce the general features of the vibrational spectra of CuOEC. However, none of these force fields reproduces the frequencies and *meso*-deuteriation shift patterns of all of the modes. All of the empirical force fields predict that the eigenvectors of certain skeletal modes are localized onto sectors of the macrocycle. This result is in general agreement with the prediction of the QCFF/PI calculations and with the data available for CuOEC, ZnOEC, and their selectively *meso*-deuteriated isotopomers presented here and in our previous work.[37,42] Quantitative comparison of the empirical and semiempirical force fields indicates that 1,4 and higher interaction constants make substantial contributions to the latter force fields. These interactions are not included in the empirical force field calculations. Accordingly, the values of the force constants used in the empirical calculations are not necessarily representative of the actual force field effective in the macrocycle. The fact that a large number of important interaction force constants are probably excluded from the empirical calculations indicates that the constraint requiring the force constants to faithfully reflect the bond lengths is necessarily artificial. Accordingly, the most important criterion for evaluating the merit of a force field should be its ability to predict accurately specific isotope shift patterns, regardless of the values of the force constants.

Acknowledgment. This work was supported by Grants GM25480 (G.T.B.), GM36243 (D.F.B.) and GM36520 (C.-K.C.) from the National Institute of General Medical Sciences.

Communications to the Editor

Photooxygenation of Chiral Allylic Alcohols: Hydroxy-Directed Regio- and Diastereoselective Ene Reaction of Singlet Oxygen

Waldemar Adam* and Bernd Nestler

Institute of Organic Chemistry
University of Würzburg, Am Hubland
D-8700 Würzburg, Germany
Received December 31, 1991
Revised Manuscript Received May 20, 1992

A recent communication,[1] in which it was quite generally stated that singlet oxygen ($^1O_2$) exhibits poor regio- and diastereoselectivity in its ene reaction with olefins, obliges us to report our preliminary results on the photooxygenation of chiral allylic alcohols **1**. In an appropriate environment, in this particular case the coordinating effect of the hydroxy group, regio- and diastereocontrol can be very high even for acyclic substrates (Table I). The directing effect of the hydroxy functionality, which is well-recognized in epoxidations by peracids[2] and transition metals[2c,d,3] and in nitrile oxide cycloadditions,[4] is novel for $^1O_2$. It permits, through its ene reaction, the introduction of a new stereogenic center with an oxygen functionality adjacent to the hydroxy group of the chiral allylic alcohol.

The by now classical cis effect[5] constitutes one of the prominent factors in controlling the regio- and stereochemistry of the prototropic ene reaction with $^1O_2$. Diastereofacial control was recently reported[5c,d,6] for a few acyclic olefins, which was attributed to the cis effect.[5]

Scheme I

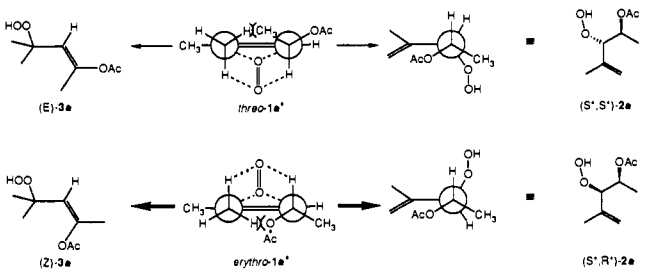

Scheme II

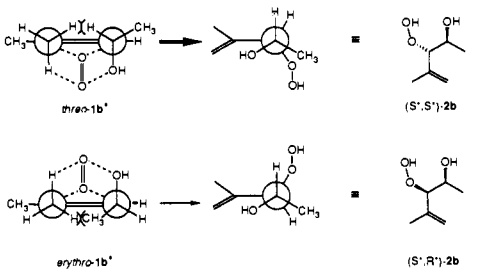

The photooxygenation of the allylic acetate **1a** (Table I, entry 1) illustrates the point under discussion (Scheme I). The pronounced regioselectivity (82:18) for **2** and **3** and moderate diastereoselectivity (d.r. = 32:68) for both (*S**,*S**)-/(*S**,*R**)-**2a** and (*E*)-/(*Z*)-**3a** can be rationalized in terms of the cis effect.[5] In fact, the same d.r. values for both sets of diastereomers demand a common transition state, namely, the perepoxide-like geometry shown in *erythro*-**1a**‡ for the major diastereomers (*S**,*R**)-**2a** and (*Z*)-**3a** and in *threo*-**1a**‡ for the minor diastereomers (*S**,*S**)-**2a**

(1) Kuroda, Y.; Sera, T.; Ogoshi, H. *J. Am. Chem. Soc.* **1991**, *113*, 2793.
(2) (a) Chautemps, P.; Pierre, J.-L. *Tetrahedron* **1976**, *32*, 549. (b) Itoh, T.; Jitsukawa, K.; Kaneda, K.; Teranishi, S. *J. Am. Chem. Soc.* **1979**, *101*, 159. (c) Rossiter, B. E.; Verhoeven, T. R.; Sharpless, K. B. *Tetrahedron Lett.* **1979**, 4733. (d) Narula, A. S. *Tetrahedron Lett.* **1981**, *22*, 2017. (e) Narula, A. S. *Tetrahedron Lett.* **1983**, *24*, 5421.
(3) (a) Narula, A. S. *Tetrahedron Lett.* **1982**, *23*, 5579. (b) Finn, G. M.; Sharpless, K. B. *Asymmetric Synthesis*; Academic Press: Orlando, FL, 1985; Vol. V, p 247.
(4) Houk, K. N.; Moses, S. R.; Wu, Y.-D.; Rondan, N. G.; Jäger, V.; Schohe, R.; Fronczek, F. R. *J. Am. Chem. Soc.* **1984**, *106*, 3880.
(5) (a) Orfanopoulos, M.; Grdina, M. B.; Stephenson, L. M. *J. Am. Chem. Soc.* **1979**, *101*, 275. (b) Schulte-Elte, K. H.; Rautenstrauch, V. *J. Am. Chem. Soc.* **1980**, *102*, 1738. (c) Adam, W.; Catalani, L. H.; Griesbeck, A. *J. Org. Chem.* **1986**, *51*, 5494. (d) Adam, W.; Nestler, B. *Liebigs Ann. Chem.* **1990**, 1051.
(6) For examples of cyclic systems, see: Adam, W.; Griesbeck, A. *Methoden der Organischen Chemie*; Houben-Weyl: Stuttgart, in press.

0002-7863/92/1514-6549$03.00/0